Intelligence-Based Medicine 12 (2025) 100264

Contents lists available at ScienceDirect

Intelligence-Based Medicine

journal homepage: www.sciencedirect.com/journal/intelligence-based-medicine

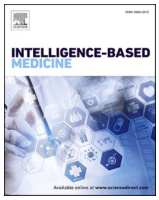

Optimizing melanoma diagnosis: A hybrid deep learning and quantum computing approach for enhanced lesion classification

Maria Frasca [a,*], Ilaria Cutica [a], Gabriella Pravettoni [a,c], Davide La Torre [b,a]

[a] University of Milan, Milan, Italy
[b] SKEMA Business School, Sophia Antipolis, France
[c] European Institute of Oncology, Milan, Italy

ARTICLE INFO

Keywords:
Melanoma
Dermatoscopic images
Quantum neural network
Medical imaging
Artificial intelligence

ABSTRACT

Melanoma is one of the most aggressive forms of skin cancer, necessitating advanced diagnostic tools to improve early detection. This study presents a novel AI-driven approach that combines deep neural networks with quantum computing techniques for enhanced lesion classification. Specifically, we employ a U-Net model for segmentation and a hybrid Convolutional Neural Network - Quantum Neural Network (CNN-QNN) for classification. Our approach achieves a precision of 99.67 %, recall of 99.67 %, and an overall accuracy of 99.35 % on the HAM10000 dataset. Additionally, we report a sensitivity of 99.4 %, a specificity of 99.2 %, and a macro F1-score of 99.5 %, significantly surpassing traditional CNN-based classifiers. This hybrid model outperforms conventional deep learning approaches, demonstrating its potential for aiding dermatologists in clinical decision-making. A comparative analysis with state-of-the-art models further validates the effectiveness of our method.

1. Introduction

The use of artificial intelligence in dermatology is an area that is attracting growing interest from both the healthcare system and companies operating in the sector. Through artificial intelligence, it is possible not only to differentiate between benign and malignant pigmented lesions, but also to improve the diagnosis and management of other dermatological conditions such as psoriasis and other inflammatory diseases, evaluate the individual characteristics of skin ulcerations, and profile gene expression. Melanoma is a serious skin cancer and its incidence is rapidly increasing in many countries. The incidence in white populations has increased by 3–5 % per year since the mid-20th century, partly due to increased sun exposure during summer months, with current rates ranging from 20 to 60 cases per 100,000 people per year [4]. Melanoma, a type of often aggressive tumor, primarily develops on the skin but can occasionally occur in the eyes or mucous membranes [1]. This cancer originates from a genetic mutation in melanocytes, the cells responsible for skin pigmentation. The incidence of skin cancer, with melanoma as its deadliest form, is steadily increasing [2]. Although traditional melanoma diagnosis relies on visual observation by dermatologists, this approach can be limited by subjectivity and the potential for human error. However, thanks to recent advances in medical technology, including automatic recognition methods and the approach to artificial intelligence (AI), there is a shift in how skin lesions are evaluated. The introduction of artificial intelligence in dermatology not only enhances the diagnosis of skin lesions but also opens new frontiers in patient care and clinical research. However, the effectiveness of AI lies not only in its diagnostic capabilities but also in its integration with clinical expertise. AI, in fact, does not replace the dermatologist but supports them in the decision-making process, reducing the risk of human error and improving the quality of care. Computer-aided diagnosis systems offer a more objective and accurate alternative. Through a series of stages, including image acquisition, lesion segmentation, feature analysis, and lesion classification, these systems aim to improve the accuracy and timeliness of melanoma diagnosis [3]. Interest in automatic melanoma recognition methods is growing as efforts are made to enhance early diagnosis effectiveness and reduce human error rates [5]. These promising developments offer new hope for quicker and more accurate melanoma diagnosis, with the potential to significantly improve treatment outcomes and patient survival prospects. Despite the advantages, the widespread adoption of AI presents significant challenges, including the need to standardize the datasets used to train the models and ensure that they are representative of diverse populations. Moreover, the use of AI raises important ethical issues, such as

* Corresponding author.
E-mail address: maria.frasca@unimi.it (M. Frasca).

https://doi.org/10.1016/j.ibmed.2025.100264
Received 26 March 2025; Received in revised form 2 May 2025; Accepted 27 May 2025
Available online 21 June 2025

protecting patient privacy and ensuring algorithmic transparency. This paper proposes a hybrid CNN-QNN architecture to leverage the strengths of classical and quantum computation. Unlike previous works that rely solely on classical deep learning, our model integrates quantum layers to enhance feature representation and classification accuracy. Our contributions are:

1. The implementation of a novel hybrid CNN-QNN model that improves melanoma classification accuracy by leveraging quantum feature mapping.
2. A systematic performance comparison between our hybrid model and conventional CNN architectures, highlighting the advantages of quantum-assisted learning.
3. A detailed analysis of the impact of the quantum layer through ablation studies, showcasing its role in boosting classification performance.
4. An exploration of statistical significance in our experimental results to ensure robustness and reliability in real-world applications.

The paper is structured as follows: Section 2 provides a detailed background on melanoma, describing the various skin lesions and associated risk factors. Section 3 examines the deep learning architectures used for the analysis of dermatological images. This includes a description of autoencoders, the U-Net network, and quantum neural networks, exploring how these technologies can be applied to the segmentation and classification of skin lesions. Section 4 highlights the existing literature on the use of artificial intelligence and deep learning in the diagnosis of skin diseases. It analyzes previous studies that have employed machine learning techniques for the segmentation and classification of skin lesions, highlighting the strengths and limitations of these approaches. Section 5 describes the HAM10000 dataset, which was used for training and validating the proposed models. The dataset contains a wide variety of skin lesion images, accompanied by detailed annotations provided by expert dermatologists. Section 6 presents the image preprocessing process, including hair removal using the Canny edge detector algorithm and autoencoders. Subsequently, the segmentation of dermatological images using the Otsu algorithm and the U-Net neural network is described. Finally, the classification of skin lesions using a quantum-classical hybrid model is illustrated. Section 7 reports the performance of the proposed models, and finally, Sections 8 and 9 highlights the benefits and limitations of the adopted methodologies. Possible directions for future improvements and research are also suggested.

2. Melanoma background

The cutaneous melanoma is a malignant tumor that originates in melanocytes, the epithelial cells responsible for melanin production, so it originates in the skin or, more rarely, in the eyes or mucous membranes [44]. Furthermore, melanocytes are responsible, under normal conditions, for the presence of dark spots on the surface of the skin known as moles, clinically defined as nevi [6]. Cutaneous melanoma can manifest on intact skin or from moles located on the skin that may be present from birth or early childhood (congenital) or appear later in life (acquired) [7]. Clinically, four types of cutaneous melanoma can be distinguished:

- ***Acral lentiginous melanoma:*** it is the rarest type of melanoma in people with fair skin and manifests at the extremities of the limbs, especially on the palms, soles, and subungual sites. This particular melanoma has a rapid intraepidermal phase, and the appearance of a nodular region reflects the onset of vertical tumor growth [8].
- ***Lentigo maligna melanoma:*** it is relatively rare (about 5–10 % of cases) and mainly occurs in elderly people; it tends to appear in sun-exposed areas damaged by chronic sun exposure and therefore mainly manifests on the face, where it takes the form of an asymmetrical, flat spot ranging from pale brown to dark brown. Its evolution is rather slow, and only in advanced stages can nodules appear on the surface [9].
- ***Nodular melanoma:*** it is a type of melanoma characterized by poor or even absent radial growth and by vertical growth from the beginning; for this reason, it is very aggressive and often presents metastases at diagnosis. It occurs in 10–15 % of cases of melanoma, especially in males around 50–60 years of age; its diagnosis is difficult as it does not give symptoms and sometimes does not present the characteristic tumor coloration [10].
- ***Superficial spreading melanoma:*** it is the most common melanoma, approximately 60–70 % of cases, and often has a biphasic course: initially, it has stable and slow horizontal growth manifested as a macular lesion; subsequently, there is a vertical growth that corresponds to an invasion depth and has an evolution of the lesion into a plaque with polychromatic or sometimes clear areas [11].

The risk of developing melanoma, a type of skin cancer, is influenced by a combination of environmental and genetic factors [12]. While sunlight exposure is often associated with melanoma, it's essential to recognize that other factors also play significant roles in its development. The interplay between genetic predisposition and environmental influences determines an individual's susceptibility to melanoma [13]. Several factors contribute to the likelihood of developing melanoma independently and significantly. Firstly, skin phototype and pigmentation are crucial. People with fair skin, light hair and eyes, as well as those with freckles (phototypes 1–2), are at a higher risk. Individuals with darker skin tones (phototype 4) generally have a lower risk compared to those with fairer complexions [14]. Family history is another important factor. If a person has a family member who has had melanoma, their own risk increases.

Around 10 % of melanoma patients have another case of the disease within their family [15]. Genetics also play a role, particularly mutations in the CDKN2A gene [16]. The likelihood of inheriting this mutation rises with the number of family members affected by melanoma. The number of moles on the body can also indicate risk. Having numerous acquired moles, especially over 100, or having 5 or more atypical moles (larger than 6 mm, irregular border, variegated color) increases the risk of developing melanoma [17]. A personal history of melanoma also increases the risk of developing another melanoma in the future. The cumulative probability of a second melanoma occurring at 5 and 10 years is notable, highlighting the importance of ongoing monitoring. Sunburn experiences during childhood and adolescence, as well as intense and intermittent sun exposure throughout life, contribute significantly to melanoma risk. Additionally, the presence of a giant congenital mole is a risk factor. These large moles present from birth can increase the likelihood of melanoma development.

It's crucial to recognize and understand these risk factors to take proactive measures. Regular skin checks and sun protection practices can aid in early detection and effective treatment of cutaneous melanoma, ultimately improving outcomes for those affected by the disease. The first step in distinguishing a mole from a melanoma is summarized in the ABCDE rule [18]:

- ***Asymmetry in shape:*** a mole is generally circular or rounded, while a melanoma has a more irregular shape.
- ***Irregular borders:*** a melanoma, unlike a benign mole, has jagged edges.
- ***Disparate color:*** moles are generally characterized by a uniform color, contrary to melanomas which have varying colors within.
- ***Diameter larger than* 6 mm:** typically, the maximum dimensions of a mole are around 6 mm in diameter, while a melanoma is characterized by development, both in width and depth.
- ***Evolution:*** unlike moles, melanomas change appearance in a relatively short time.

Other warning signs that should be evaluated by a doctor are a mole that bleeds, itches, or is surrounded by a lump or a reddened area. The presence of all these characteristics facilitates the recognition and diagnosis of a melanoma. However, when the melanoma is in the early stages or when only some clinical characteristics of the ABCDE are found in a mole, the diagnosis can be challenging [1]. The difficulty of clinical evaluation can lead to both a high rate of unnecessary mole removals and an underestimation of the diagnosis. For this reason, in order to increase diagnostic sensitivity, the specialist may resort to the use of tools that allow better observations than direct naked-eye observation [19].

3. Deep learning architectures: a review

We now provide an overview of the key properties of the deep learning architectures employed in the remainder of this paper. For additional details one can refer, for instance, to Refs. [20,53,54].

3.1. Autoencoder architecture

Autoencoders [21] are a type of artificial neural network designed to learn a compact and meaningful representation of data, typically used for unsupervised learning. Autoencoders find numerous applications, such as dimensionality reduction, where the goal is to compress data into a reduced latent space, image denoising, where autoencoders are used to remove noise from data, and anomaly detection, in which significant deviations between the input and the reconstruction indicate potential anomalies. Their architecture consists of two main components: the encoder and the decoder [22].

- ***Encoder***: The encoder maps the high-dimensional input, typically represented as a vector $\mathbf{x} \in \mathbb{R}^n$, into a lower-dimensional space, called the latent space or latent code $\mathbf{z} \in \mathbb{R}^m$, where $m < n$. Mathematically, this transformation can be expressed as:

$$\mathbf{z} = f(\mathbf{x}) = \sigma(\mathbf{W}_e\mathbf{x} + \mathbf{b}_e) \tag{1}$$

  where $\mathbf{W}_e$ is the encoder's weight matrix, $\mathbf{b}_e$ is the bias, and σ is a nonlinear activation function (such as ReLU or sigmoid).
- ***Decoder:*** The encoder maps the high-dimensional input, typically represented as a vector $\mathbf{x} \in \mathbb{R}^n$, into a lower-dimensional space, called the latent space or latent code $\mathbf{z} \in \mathbb{R}^m$, where $m < n$. Mathematically, this transformation can be expressed as:

$$\mathbf{z} = f(\mathbf{x}) = \sigma(\mathbf{W}_e\mathbf{x} + \mathbf{b}_e) \tag{2}$$

  where $\mathbf{W}_e$ is the encoder's weight matrix, $\mathbf{b}_e$ is the bias, and σ is a nonlinear activation function (such as ReLU or sigmoid).

The goal of the autoencoder is to minimize the difference between the input $\mathbf{x}$ and its reconstruction $\hat{\mathbf{x}}$. This difference is measured using a loss function, commonly the Mean Squared Error (MSE). The learning process of autoencoders involves optimizing the weights $\mathbf{W}_e$ and $\mathbf{W}_d$, and the biases $\mathbf{b}_e$ and $\mathbf{b}_d$, using optimization algorithms such as Adam or Stochastic Gradient Descent (SGD). The optimization process aims to minimize the loss function $L(\mathbf{x}, \hat{\mathbf{x}})$, improving the model's ability to faithfully reconstruct the input [23].

3.2. U-Net architecture

As depicted in Fig. 1, the U-Net model exhibits a fairly symmetrical architecture, with a contraction part on the left mirroring roughly the expansion part on the right, hence the "U" shape. Moreover, both the expansion and contraction phases consist of four levels. The contraction part comprises, for each phase, two convolutional layers followed by a max-pooling layer to decrease dimensions. With each contraction phase, the number of image channels doubles. In the expansion part, for each phase, there exists a layer for up-convolution, taking low-resolution images as input and producing higher resolution ones, along with two convolutional layers. At each expansion phase, the number of channels halves. The output from the network's contraction path is concatenated to each up-convolution layer. Finally, at the end of the expansion phase, a convolutional layer is added to create the feature map within the desired classes [24].

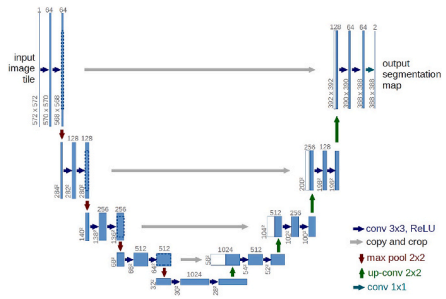

Fig. 1. The U-Net architecture used for dermatological image segmentation. The structure consists of a contraction path (encoder) for feature extraction and an expansion path (decoder) for segmentation reconstruction. Skip connections help preserve image details.

3.3. Quantum neural network

Quantum neural networks (QNNs) are an innovative fusion of quantum theory and traditional neural networks. These models, systems, or devices combine the characteristics of quantum mechanics with the properties of neural networks, which are models of interconnected units inspired by the functioning of biological neurons. In the context of quantum neural networks, neurons are conceived as qubits, which are quantum processing units that can simultaneously represent 0 and 1 thanks to the principle of quantum superposition. This theoretical approach paves the way for a new form of information processing, where concepts from quantum physics are leveraged to enhance the capabilities of neural networks in learning and data processing. Essentially, quantum neural networks harness the power of quantum mechanics to improve the performance of traditional neural networks, offering new opportunities to solve complex problems in fields such as pattern recognition, optimization, and cryptography [25]. In the case of quantum neural networks (QNNs), the process of neuron operations is significantly different from classical neural networks.

In classical neural networks, information processing occurs through classical bits, while in quantum neural networks, qubits or quantum bits are used [25]. The field of quantum computing, including quantum neural networks, is still in its early stages and faces significant technical challenges [26]. In a classical neuron, the output is determined by applying an activation function to the weighted sum of the inputs, adding a bias term. This is expressed by the following formula:

$$\text{Output} = \text{Activation}\left(\sum_i w_i x_i + b\right) \tag{3}$$

where w_i represents the weight associated with the input x_i, and b is the bias, while *Activation* is the activation function. As for the quantum neuron, it utilizes quantum states to represent information and applies quantum gates to perform computations. This is expressed by the following formula:

$$|\psi_{\text{out}}\rangle = U(\theta)|\psi_{\text{in}}\rangle \tag{4}$$

Where, $U(\theta)$ is a quantum gate parameterized by θ), and ψ_{in} and ψ_{out} are the input and output quantum states, respectively. Quantum layers are essential components of QNNs. In a quantum layer, qubits encode information, and a series of quantum gates perform operations on these

qubits. These gates exploit quantum phenomena such as superposition and entanglement, allowing for parallel information processing. Quantum states are manipulated through a set of quantum gates, and the resulting quantum information is often measured to obtain a classical output. The challenge lies in mitigating issues such as quantum decoherence and errors. The classical output can be used as feedback to adjust the parameters of the quantum gates in subsequent layers, contributing to the learning process [27].

The classical layers in classical neural networks are composed of layers of interconnected neurons:

$$\text{Layer}_{\text{out}} = \text{Activation}(\text{Layer}_{\text{in}} \cdot \text{Weights} + \text{Biases}) \tag{5}$$

The quantum layer in QNNs has quantum layers composed of quantum neurons.

$$|\psi_{\text{out}}\rangle = U(\theta_n)U(\theta_{n-1})\ldots U(\theta_1)|\psi_{\text{in}}\rangle \tag{6}$$

where $U(\theta_1)$ is the quantum gate in the i-th neuron. Training the quantum circuit involves updating the parameters of the quantum gates in response to a loss function:

$$\theta_{\text{new}} = \theta_{\text{old}} - \eta \cdot \nabla_\theta L_{\text{loss}} \tag{7}$$

where θ_{old} and θ_{new} re the old and updated parameters, respectively, η s the learning rate, and $\nabla_\theta L_{\text{loss}}$ is the gradient of the loss with respect to the parameters [28].

3.3.1. Convolutional neural networks-quantum neural networks

Hybrid CNN-QNN neural networks (Convolutional Neural Networks - Quantum Neural Networks) combine elements of classical convolutional neural networks (CNNs) with quantum neural networks (QNNs), aiming to leverage the strengths of both technologies to enhance data processing and analysis capabilities. In a hybrid CNN-QNN network, the initial convolutional models are used to extract features from images in a classical way, and then these results are passed to a quantum component for further processing. Specifically, the CNN handles feature extraction, transforming complex data into simpler, more compact representations, which can then be processed by the quantum neural network [29]. The QNN utilizes quantum computational power to analyze these representations and make more accurate or faster decisions. The main operations are shown below:

- ***Convolution Operations***: The convolution of an image I with a filter K of size $m \times n$ is defined as:

$$S(i,j) = \sum_{k=0}^{m-1}\sum_{l=0}^{n-1} I(i+k, j+l)\cdot K(k,l) \tag{8}$$

where:
- I is the input image.
- K is the kernel (filter) applied to the image.
- $S(i, j)$ is the result of the convolution at position (i, j).

The output of the CNN, represented by a vector of numerical features extracted from the images, is prepared for quantum processing through dimensionality reduction and a dedicated mapping process. Each value in this vector is transformed into a rotation angle $R_Y(\theta)$, encoding the information into the qubits of the quantum circuit. The circuit then applies quantum gates, such as the CNOT gate, to create entanglement between qubits, leveraging the properties of quantum mechanics to establish complex correlations among the variables. After measuring the states along the Z-axis, the results are returned to the classical domain as a set of values seamlessly integrated into the final dense layers to complete the classification process. To ensure effective training, the entire system employs an optimization strategy that combines classical and quantum techniques. The CNN uses the Adam algorithm for rapid and stable weight updates, while the quantum component leverages the parameter-shift rule to compute the gradients needed for optimizing the circuit's parameters. This synergy allows the model to be trained end-to-end, simultaneously optimizing both components to ensure robust and precise data processing.

- ***Quantum Operations***: Quantum neural networks use operations on qubits. A common operation is the rotation of a qubit around the Y axis, represented as:

$$R_Y(\theta) = \begin{bmatrix} \cos(\theta/2) & -\sin(\theta/2) \\ \sin(\theta/2) & \cos(\theta/2) \end{bmatrix} \tag{9}$$

where θ is the rotation angle of the qubit.

- ***Entanglement via CNOT***: Entanglement between two qubits can be implemented with a CNOT gate:

$$\text{CNOT} = \begin{bmatrix} 1 & 0 & 0 & 0 \\ 0 & 1 & 0 & 0 \\ 0 & 0 & 0 & 1 \\ 0 & 0 & 1 & 0 \end{bmatrix} \tag{10}$$

This operation creates quantum correlations between the qubits.

An example of a CNN-QNN hybrid network is shown in Fig. 2.

4. Related work

AI techniques are transforming melanoma diagnosis. These methods analyze dermatological images to identify malignant lesions with high precision, often surpassing the capabilities of human dermatologists. Adegun et al. [30] describe the use of a deep learning-based system for automatic melanoma detection. Utilizing CNNs, the system analyzes dermoscopic images to identify malignant lesions with high precision. Techniques such as data augmentation, transfer learning, and image preprocessing are employed to enhance model performance. The model is trained on large datasets of dermatological images, significantly improving its ability to detect melanoma compared to traditional methods. The results show an accuracy exceeding 90 %, highlighting the potential of deep learning to improve early diagnosis and reduce misdiagnoses. Seeja et al. describe an approach that combines CNNs for skin lesion segmentation and Support Vector Machines (SVM) for classification. The CNN is used to accurately segment lesions from dermoscopic images, while the SVM classifies the lesions as benign or malignant. The results show a segmentation accuracy of 94 %, classification accuracy of 92 %, precision of 91 %, sensitivity of 90 %, and specificity of 89 %. This combined approach demonstrates improved melanoma diagnosis compared to traditional methods. Daghrir et al. [31] present an innovative method combining deep learning and traditional machine learning techniques to improve melanoma diagnosis. Utilizing CNNs to extract features from dermoscopic images and algorithms like SVM and Random Forest for classification, the hybrid approach showed promising results. It achieved an accuracy of 95 %, precision of 93 %, sensitivity of

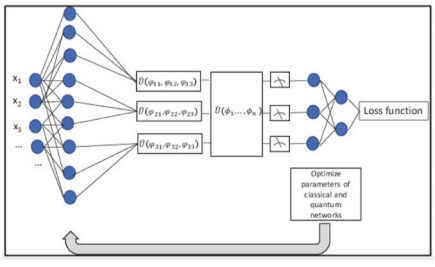

Fig. 2. Schematic representation of the hybrid CNN-QNN neural network used for skin lesion classification. The model combines a CNN for feature extraction with a quantum neural network to enhance data representation and generalization.

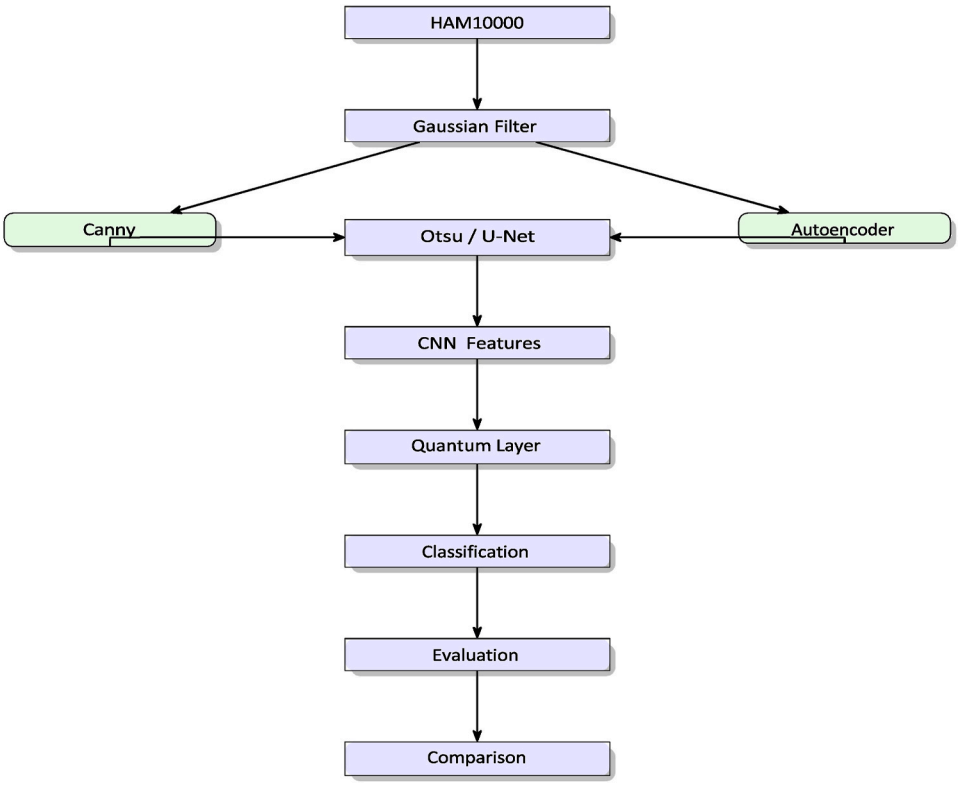

Fig. 3. Compact block diagram of the proposed CNN-QNN pipeline for melanoma classification, showing preprocessing, segmentation, feature extraction, quantum mapping, and final prediction.

92 %, and specificity of 90 %. These results demonstrate that the hybrid approach can provide more accurate diagnoses, significantly reducing misdiagnoses and improving the clinical management of melanoma. Acosta et al. [32] use deep learning techniques to improve melanoma diagnosis. Employing Mask R-CNN for lesion segmentation and ResNet152 for classification, the system achieved a segmentation accuracy of 94 %, classification accuracy of 92 %, precision of 91 %, sensitivity of 90 %, and specificity of 89 %. These results demonstrate that deep learning can effectively identify malignant lesions, surpassing traditional methods and reducing misdiagnoses. Hussain et al. [33] aim to improve nail melanoma diagnosis using quantized deep-learning models based on transfer learning. Utilizing annotated nail image datasets, the models achieved over 95 % accuracy while maintaining computational efficiency through quantization. This approach allows for implementation on mobile devices, making the technology accessible for real-time clinical applications and enhancing early diagnosis and clinical management of nail melanoma. Sivakumar et al. [34] explore the use of deep learning for skin lesion analysis and malignant melanoma identification. Utilizing CNNs such as VGG16 and ResNet50, the system analyzes dermatological images to segment and classify lesions. The results show a classification accuracy of 93 %, precision of 91 %, sensitivity of 90 %, and specificity of 88 %. Lopez et al. [35] explore the integration of quantum computing in the diagnosis of melanoma. Using CNNs such as U-Net for segmentation and ResNet for classification, optimized through quantum algorithms like Quantum Approximate Optimization Algorithm (QAOA) and Variational Quantum Eigensolver (VQE), the system significantly improves skin lesion segmentation and classification. The results show a segmentation accuracy that exceeds 96 % and a classification accuracy of 94 %, demonstrating the potential of quantum techniques to improve the early diagnosis and treatment of melanoma.

Li et al. [36] describe an approach that integrates quantum computing with the Inception-ResNet-V1 architecture to classify multi-class skin damage images. By utilizing quantum algorithms to optimize the classification process, the system improves accuracy and efficiency compared to traditional methods. The results indicate a classification accuracy of over 95 %, highlighting the impact of quantum technologies in enhancing diagnostic capabilities in dermatology.

Razmjooy et al. [37] describes an innovative approach for skin melanoma segmentation. Utilizing CNNs such as U-Net and Fully Convolutional Network (FCN) optimized by the Quantum Invasive Weed Optimization (QIWO) algorithm, the system improves skin lesion segmentation compared to traditional methods. The results show a segmentation accuracy of over 95 %, demonstrating that the integration of quantum optimization techniques can significantly enhance the performance of deep learning models in melanoma diagnosis. Ciccincione et al. [38] describe the use of Transformer models for melanoma detection in dermoscopic images. Utilizing the Transformer architecture, known for its success in natural language processing, the system analyzes and classifies skin lesion images. The results indicate that the Transformer-based approach improves diagnostic accuracy compared to traditional models, achieving a classification accuracy of over 96 %. This method offers new possibilities for early and precise melanoma diagnosis.

Recent studies have highlighted the increasing role of hybrid quantum-classical approaches in enhancing medical image analysis. For instance, in Ref. [46], the integration of quantum layers within classical deep learning architectures is shown to improve pattern recognition and classification capabilities, supporting our decision to incorporate a QNN component. Similarly, the application of quantum neural networks to real-world biomedical tasks, as discussed in Refs. [47,48], validates the potential of quantum computing in clinical contexts.

Moreover, optimization of neural architectures remains a key challenge in deep learning, particularly in medical domains where model efficiency is crucial. The bio-inspired optimization strategies presented in Ref. [51] offer insights that could be adapted to refine preprocessing or feature extraction stages in dermatological imaging.

From a broader perspective, the works in Refs. [50,52] emphasize

the importance of scalability and interpretability in AI-driven diagnostics. These aspects align with the challenges identified in our study, particularly regarding the computational cost of simulating quantum circuits and the need for transparent model outputs in clinical practice.

5. Dataset

The dataset used was the HAM10000 (”Human Against Machine with 10.000 training images”), is a large collection of data containing images of skin lesions from patients with various dermatological conditions [39]. This dataset was created with the aim of providing a valuable resource for research in the field of computational dermatology and artificial intelligence applied to the diagnosis of skin diseases. The composition of the dataset includes various types of skin lesions, including:

- ***Nevi:*** Images of benign moles, which are common skin lesions and generally non-cancerous.
- ***Melanomas:*** Images of melanomas, which are a type of skin cancer derived from melanocytes, are particularly important for the study of early diagnosis and treatment of the disease.
- ***Actinic keratoses:*** These skin lesions, commonly called ”sunspots,” are precancerous and can progress to squamous cell carcinoma if left untreated.
- ***Angiomas:*** Images of angiomas, which are benign vascular formations.
- ***Other benign and malignant skin lesions:*** The dataset also includes other dermatological conditions such as warts, seborrheic keratoses, dermatitis, and other common skin lesions.

Each image in the dataset is accompanied by detailed annotations provided by expert dermatologists. These annotations include information about the clinical characteristics of the lesions, such as size, shape, asymmetry, irregular borders, color variations, and other features relevant to the diagnosis and classification of skin lesions. The predominant part of the dataset is composed of images of melanocytic nevi (nv 6.705), benign lesions similar to keratosis (bkl 1.099) and melanomas (mel 1.113).

Additionally, the HAM10000 dataset also includes clinical metadata associated with each image, such as patient age, gender, lesion location, and any previous clinical diagnoses.

The diverse and detailed composition of the HAM10000 dataset makes it a valuable resource for research in the field of computational dermatology and artificial intelligence applied to the diagnosis and treatment of skin diseases.

6. Methodology

To facilitate a clearer understanding of the overall proposed methodology and to clearly highlight the different operational phases adopted in this study, a synthetic block diagram has been created 3.

This diagram clearly illustrates the work’s innovative contribution, consisting of the combination of classical techniques and quantum computing applied to automated diagnostic support for melanoma.

6.1. Pre-processing and hair removal

Preprocessing of dermoscopic images is crucial to ensure the quality and accuracy of automated analysis and diagnosis of skin lesions. For preprocessing, we applied the Gaussian filter for noise removal. The Gaussian filter is a convolutional mask based on the Gaussian function that improves the visual quality of the image, facilitating subsequent analyses. The image is convolved with the Gaussian mask, which smooths the image by attenuating high frequencies, reducing high-frequency noise without significantly altering the main details. Although the Gaussian filter effectively reduces noise, it can also slightly blur the edges. We applied the Canny Edge Detection algorithm to minimize this effect for edge refinement after convolution. For hair removal from dermoscopic images, we applied two processes: the Canny algorithm and an autoencoder architecture.

6.1.1. Canny edge detection algorithm

For hair removal from dermatoscopic images with the Canny edge detection algorithm, we reduced noise in the image by first applying a Gaussian filter (kernel size $= 5 \times 5$, sigma $= 1.5$) to smooth the image and remove high-frequency noise. We then computed intensity changes to identify edges, removed pixels that do not represent main edges, and applied dual-threshold hysteresis (low threshold $= 50$, high threshold $=$ 150) to distinguish strong from weak edges. Specifically, Canny edge detection occurs in two main stages: in the first stage, light and dark hairs are segmented using an adaptive Canny edge detector and refined with morphological closing operations (structuring element $= 3 \times 3$) to ensure continuity in detected structures. In the second stage, hairs are repaired using a coherence-based retouching technique at various resolutions, ensuring smoother texture reconstruction. This multi-resolution approach significantly enhances image quality, making it easier to accurately diagnose skin lesions (see Fig. 3).

The hair removal process includes several steps. First, noise reduction with a Gaussian filter (5×5, sigma $= 1.5$) is applied, which attenuates high frequencies while preserving essential image details. Next, the image is converted to grayscale to facilitate segmentation. We enhance contrast using adaptive histogram equalization to improve the differentiation between hair and skin regions. Hair segmentation is performed using Otsu’s thresholding, which dynamically calculates an optimal threshold to separate hairs from the background, creating a binary mask where hairs are represented by white pixels on a black background. Following segmentation, morphological operations are used to remove isolated noise and refine the mask. After segmentation, inverting the colors of the binary mask improves the visibility of the hairs, making them black on a white background. This inversion makes it easier to identify hairs in the original image. The next step involves using the mask to remove hair from the original image through image inpainting techniques based on coherence diffusion, where hair pixels are replaced with interpolated values from surrounding skin regions. To further enhance this process, we use a GAN-based inpainting model trained on dermoscopic datasets to predict and restore occluded regions with realistic skin textures. The combined process of Gaussian filtering, edge detection, threshold-based segmentation, morphological refinement, and coherence-based inpainting ensures that hairs are effectively removed from the dermatoscopic image, as shown in Fig. 4.

6.1.2. Autoencoder architecture for hair removal

The first step in the process is preprocessing the images to separate the hair from the skin. This is achieved by converting the image to grayscale and applying an intensity threshold (set to 100) to create a binary mask that distinguishes the hair (dark areas) from the rest of the image. The binary mask is then inverted to isolate the hair and applied to the original image to remove the corresponding hair regions, filling them with a uniform background color, typically white. Subsequently, the autoencoder is defined to learn to reconstruct the original image without hair. The autoencoder is composed of encoder and decoder blocks: the encoder reduces the dimensionality of the image and extracts its main features, while the decoder uses these features to reconstruct the original image. To improve reconstruction accuracy, we integrate skip connections between encoder and decoder layers, ensuring that fine details are preserved.

- *EncoderBlock 1:* Reduces the image from 3 channels (RGB) to 128 channels.
- *EncoderBlock 2:* Further reduces it from 128 to 256 channels.

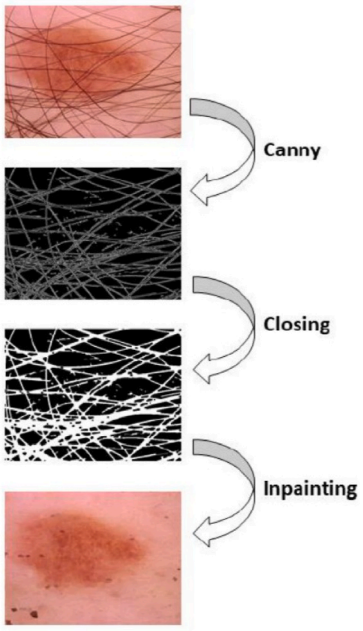

Fig. 4. Application of the Canny edge detection algorithm for hair removal in dermoscopic images. The process occurs in two steps: edge detection followed by interpolation to fill in the removed areas. This enhancement allows for more accurate segmentation.

The decoder, on the other hand, uses these features to reconstruct the original image without hair:

- *DecoderBlock 1:* Expands the image from 256 channels to 128 channels, using skip connections that concatenate data from the encoder to enhance the reconstruction.
- *DecoderBlock 2:* Reconstructs the final image in 3 channels (RGB), aiming to reproduce the color fidelity and structural coherence of the original image.

The learning process is guided by a highly customized loss function that combines various terms, such as L1 Loss, L2 Loss, SSIM Loss, and TV Loss. These terms help optimize different aspects of the reconstructed image: color fidelity, structural coherence, and spatial regularity. To further improve performance, we apply data augmentation techniques such as random rotations and brightness adjustments to increase generalization. After training, the model is capable of generating hairless skin images with high fidelity to the original image, preserving essential details and minimizing distortions introduced by hair removal, as shown in Fig. 5.

6.2. Segmentation

The segmentation of dermatoscopic images represents a crucial aspect of automated analysis of skin lesions, as it allows for the precise isolation of regions of interest, such as lesions, from the surrounding tissue [40]. This process is fundamental in supporting accurate diagnosis, especially in skin diseases like melanoma, where distinguishing between healthy and malignant tissues is essential. Automated segmentation utilizes advanced algorithms capable of learning and recognizing complex patterns of color, shape, and texture present in dermatoscopic images. These algorithms can identify critical features, such as irregular margins, asymmetries, and color variations, which are typical signs of malignant lesions [41]. Accurate segmentation is particularly important not only for the initial diagnosis but also for monitoring lesions over time, enabling dermatologists to assess their evolution and make more informed therapeutic decisions.

The automated segmentation of dermatoscopic images is made complex by several technical challenges. Dermatoscopic images are often subject to significant variability in terms of lighting, contrast, and quality, which can interfere with the accuracy of the segmentation. For the segmentation in our article, we used the Otsu algorithm and the UNet neural network.

6.2.1. Otsu algorithm

The Otsu method is a widely used global thresholding technique that determines an optimal threshold by minimizing intra-class variance. It provides a simple and computationally efficient way to segment dermatoscopic images. However, it is sensitive to illumination changes and lacks the adaptability required for complex skin lesions. To enhance robustness, we incorporated a pre-processing step that includes Gaussian smoothing (kernel size $= 5 \times 5$) to reduce noise before applying the Otsu method.

The first step in the segmentation process is converting the image from a color format (BGR) to grayscale. After converting to grayscale, the image is passed through a median filter using a 5×5 window. This filter effectively reduces noise while preserving sharp edges in the

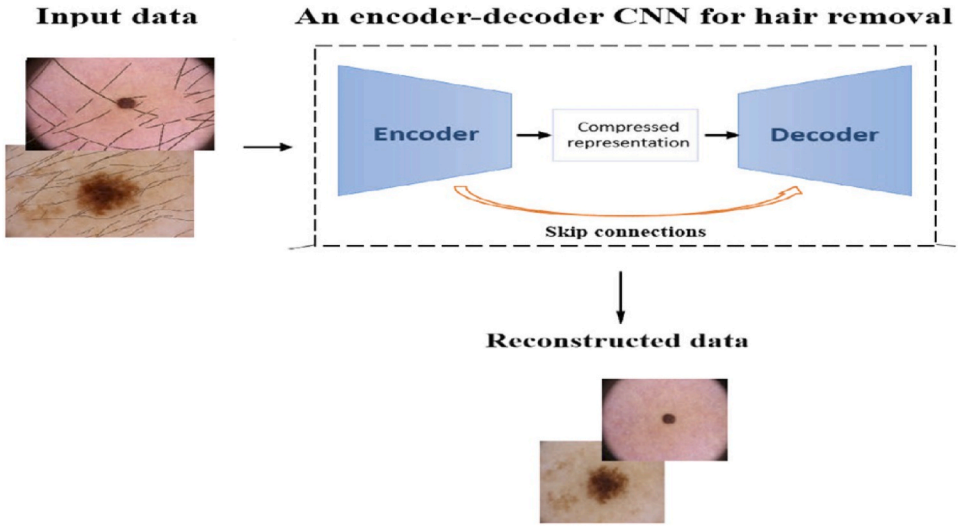

Fig. 5. Results obtained using an Autoencoder architecture for hair removal in dermoscopic images. The autoencoder learns a latent representation of the image and reconstructs a version without interference, improving segmentation quality.

structures present in the image. Next, an adaptive thresholding technique is applied to generate a binary mask. Unlike global thresholding methods that apply the same threshold across the image, this adaptive threshold dynamically adjusts based on local intensity variations, making it particularly useful for dermoscopic images with uneven lighting conditions. To further refine this step, we integrated a local contrast enhancement method before thresholding, improving lesion-background separation. Once the binary mask is created, colors are inverted, ensuring lesions (or areas of interest) appear white while the background remains black. This enhances the segmentation's visibility and facilitates further analysis. To restore original color details in the segmented regions, we apply a *bitwise$_a$nd* operation, allowing the original lesion details to be retained while removing unwanted background noise. Additionally, we employ a morphological closing operation (kernel size $= 3 \times 3$) to refine the lesion shape and reduce artifacts in the binary mask. This approach significantly improves segmentation quality, as illustrated in Fig. 6.

6.2.2. UNet neural network

In this segmentation process using UNet, the images are resized to 128×128 pixels and converted to grayscale to simplify processing. Additionally, brightness enhancement with a factor of 1.5 is applied using the 'ImageEnhance.Brightness' class from the PIL library. This step aims to make the features of the skin lesions more prominent in the images, facilitating the segmentation task for the model. The U-Net network consists of several convolutional layers, organized into an encoding path (encoder) and a decoding path (decoder), connected by a "bottleneck." The structure of the network is as follows:

- **Input Layer:** Input shape: (128, 128, 1) (grayscale image).
- **Encoding Path (Encoder):**
  - **Conv1:** Two convolutional layers with 64 filters, 3×3 kernel size, ReLU activation, and padding. These layers extract the initial features from the image.
  - **MaxPooling1:** Pooling operation with a 2×2 window, reducing the spatial dimension of the features by a factor of 2.
  - **Conv2:** Two convolutional layers with 128 filters, 3×3 kernel size, ReLU activation, and padding.
  - **MaxPooling2:** Pooling with a 2×2 window.
  - **Conv3:** Two convolutional layers with 256 filters, 3×3 kernel size, ReLU activation, and padding.
  - **MaxPooling3:** Pooling with a 2×2 window.
  - **Conv4:** Two convolutional layers with 512 filters, 3×3 kernel size, ReLU activation, and padding.
  - **MaxPooling4:** Pooling with a 2×2 window.
- **Bottleneck:**
  - **Conv5:** Two convolutional layers with 1024 filters, 3×3 kernel size, ReLU activation, and padding. This is the deepest layer of the network, where highly abstract representations of features are learned.
- **Decoding Path (Decoder):**
  - **Up6:** Upsampling operation with a factor of 2, followed by concatenation with the features from Conv4 (skip connection), followed by two convolutions with 512 filters, 3×3 kernel size, ReLU activation, and padding.
  - **Up7:** Upsampling with a factor of 2, concatenation with the features from Conv3, followed by two convolutions with 256 filters.
  - **Up8:** Upsampling with a factor of 2, concatenation with the features from Conv2, followed by two convolutions with 128 filters.
  - **Up9:** Upsampling with a factor of 2, concatenation with the features from Conv1, followed by two convolutions with 64 filters.
- **Output Layer:**
  - A convolutional layer with 1 filter, 1×1 kernel size, and sigmoid activation. This layer generates a binary probability map indicating the presence or absence of lesions in each pixel of the image.

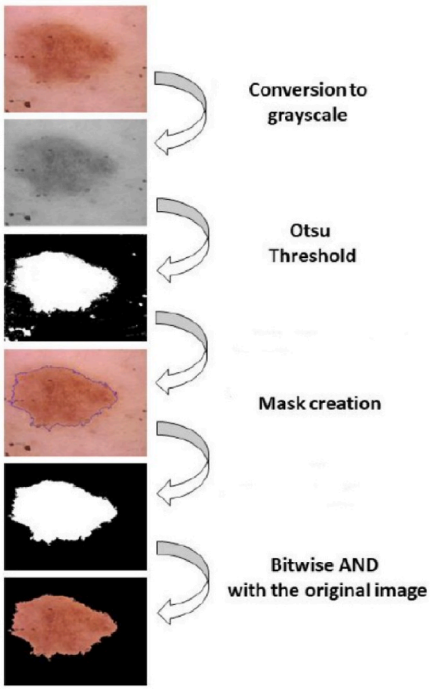

Fig. 6. Results of segmentation using the Otsu algorithm. The original image is converted to grayscale, and an optimal threshold is computed to separate the lesion from the background. This method is effective for images with high contrast but may be limited under varying lighting conditions.

The U-Net model is compiled using the Adam optimizer, known for its efficiency in quickly converging during training. The loss function used is binary_crossentropy, suitable for binary segmentation, where each pixel is classified as lesion or non-lesion. The model was trained for 100 epochs with a batch size of 32 using the training data, while performance was evaluated on a separate validation set to prevent overfitting. After training, the model was used to segment the images in the test set. The segmented masks are generated by applying a threshold to the network output, with a threshold value set at 32 to highlight finer lesions. These masks are then superimposed on the original color images, restoring the colors in the segmented areas, as shown in Fig. 7.

6.3. Classification

For the classification, we used a simulation of a quantum neural network (QuantumNet) [42]. Training a real quantum neural network on a normal classical computer is not possible, as an authentic quantum neural network requires the use of qubits and access to a quantum computer to perform quantum operations. However, there are some approaches that allow the simulation of quantum neural networks on classical computers. The specifications of our PC are:

- HP Zbook Fury 17 G7 Mobile workstation computer;
- High-level NVIDIA Quadro RTX 3000 GPU;
- Windows 11 Pro 64-bit operating system;
- Core i9-10885H CPU with 2.40 GHz processor speed.

Fig. 7. Process for the lesion segmentation and extraction with Unet

We implemented a hybrid quantum-classical model using a convolutional neural network architecture integrated with a simulated quantum circuit. The images were resized to 128 × 128 pixels and converted to grayscale. This resizing is essential to ensure that all images have the same dimensions and can be processed. The classical part of the network includes:

- **Convolutional Layers:**
  - **Conv1:** First convolutional layer with 16 filters, a 3 × 3 kernel size, stride of 1, and padding of 1. This layer extracts low-level features from the image, such as edges and textures.
  - **Conv2:** Second convolutional layer with 32 filters, a 3 × 3 kernel size, stride of 1, and padding of 1. It increases the complexity of the extracted features.
  - **Conv3:** Third convolutional layer with 64 filters, a 3 × 3 kernel size, stride of 1, and padding of 1. Extracts high-level features.
  - **MaxPooling:** A 2 × 2 pooling operation is applied after Conv2 and Conv3, reducing the spatial dimensionality of the input images while retaining the most important features.
  - **Flattening:** After the last convolutional layer, the output is flattened into a vector of size 64 × 32 × 32 to be passed through the subsequent dense layers.
- **Quantum Component:**
  - **Quantum Layer:** The quantum layer is implemented through a simulated quantum circuit defined in the `quantum_circuit` function. This circuit receives as input a feature vector of size `n_qubits` (4 in our case). Each value of the vector is mapped onto an RY rotation on each qubit. CNOT operations are applied to create entanglement between the qubits. The weights `q_params`, initialized randomly, are optimized during training.
  - **Quantum Output:** The output of the quantum circuit consists of the expectations of the qubits measured along the Z axis (PauliZ), which is subsequently converted into a PyTorch tensor for use in the subsequent dense layers of the neural network.
- **Dense Layers:**
  - **FC1:** Dense layer that takes as input the output of the convolutional network (flattened into a vector) and maps it to a space of size `n_qubits` (4 qubits). This vector is then passed through the quantum circuit.
  - **FC2:** Dense layer that maps the output of the quantum circuit (of size 4) to 128 units.
  - **FC3:** Final output layer that maps the 128 units to the predicted output classes (`n_classes`), using a softmax activation function.

The model optimization was carried out using the Adam algorithm, which is chosen for its efficiency in handling gradient descent. Adam adjusts the learning rate for each parameter during training, contributing to faster and more stable convergence. In our case, the learning rate was set to 0.001, a value carefully chosen to balance the speed of learning with the stability of training. To identify the optimal learning rate for our CNN-QNN model, we tested several configurations, including 0.01, 0.001, and 0.0001. The results demonstrated that 0.001 provided the best trade-off: it ensured stable and rapid convergence without the oscillations observed at higher values like 0.01, while significantly reducing training time compared to lower values such as 0.0001. Regarding the loss function, CrossEntropyLoss was used, which is appropriate for multi-class classification problems. This loss function measures the distance between the probability distribution predicted by the model and the actual distribution of the labels, penalizing incorrect predictions. The model was trained for 100 epochs, where it learned from the training images and updated its parameters to improve its predictive accuracy. Additionally, we utilized the k-fold cross-validation technique with $k = 5$, allowing the model's performance to be assessed across multiple data subsets. This approach helped to prevent overfitting and enhance generalization.

7. Results

The results obtained for the segmentation with the UNet neural network are shown in Table 1 2 3.

To evaluate the performance of the QuantumNet model, we calculated the following metrics [43]:

- ***Macro Averaged Accuracy.*** This metric is calculated as the average accuracy across all classes. Initially, the accuracy for each class k is determined individually:

$$Accuracy_k = \frac{TP_k}{TP_k + TN_k} \tag{11}$$

After that, the overall average of these accuracy values is computed:

$$MAAccuracy = \frac{\sum_{k=1}^{K} Accuracy_k}{K} \tag{12}$$

- ***Macro Averaged Precision.*** To compute this metric, the precision for each class k is first calculated separately:

$$Precision_k = \frac{TP_k}{TP_k + FP_k} \tag{13}$$

Then, the average precision across all classes is determined:

$$MAPrecision = \frac{\sum_{k=1}^{K} Precision_k}{K} \tag{14}$$

- ***Macro Averaged Recall.*** This metric is computed by first determining the recall for each class k:

$$Recall_k = \frac{TP_k}{TP_k + FN_k} \tag{15}$$

Subsequently, the average recall across all classes is calculated:

$$MARecall = \frac{\sum_{k=1}^{K} Recall_k}{K} \tag{16}$$

- ***Macro Averaged F1.*** The F1 score is the harmonic mean of precision and recall. This score is calculated as follows:

$$Macro\_F1 = 2 \times \frac{Macro\_Precision \times Macro\_Recall}{Macro\_Precision + Macro\_Recall} \tag{17}$$

- ***Macro Averaged OVR AUC.*** This metric measures the model's ability to distinguish between each class (One Versus Rest). To obtain this, the AUC for each class's ROC curve is computed, and the average across all classes is taken.

The comparison with other models, including traditional CNN architectures, ResNet, and SOM, has been thoroughly explored in previous

Table 1
Dataset HAM 10000 without hair removal.

Metrics	Original Dataset	Otzu Segmentation	U-Net Segmentation
Accuracy	73.09 % 73.09	%	78.07 %
Precision	53.42 %	53.42 %	73.14 %
Recall	73.09 %	73.09 %	78.07 %
F1 Score	61.72 %	61.72 %	73.46 %
AUC	48.57 %	42.17 %	85.64 %

Table 2
Dataset HAM 10000 with Autoencoder Neural Network hair removal.

Metrics	Original Dataset	Otzu Segmentation	U-Net Segmentation
Accuracy	73.09 %	73.09 %	99.67 %
Precision	53.42 %	53.42 %	99.35 %
Recall	73.09 %	73.09 %	99.67 %
F1 Score	61.72 %	61.72 %	99.51 %
AUC	52.97 %	63.87 %	99.76 %

Table 3
Dataset HAM 10000 with Canny Algorithm hair removal.

Metrics	Original Dataset	Otzu Segmentation	U-Net Segmentation
Accuracy	73.09 %	73.09 %	98.37 %
Precision	53.42 %	53.42 %	98.15 %
Recall	73.09 %	73.09 %	98.37 %
F1 Score	61.72 %	61.72 %	98.21 %
AUC	48.60 %	50.13 %	98.68 %

studies as [5,19,45,49]. In this analysis, we have focused on a detailed evaluation of performance metrics to provide a more comprehensive assessment of the effectiveness of the proposed model.

Specifically, using the same image preprocessing and segmentation pipeline, we compared the performance of the CNN-QNN model with ResNet-50. The results showed in Fig. 8 and in Table 4 that:

- Explained Variance by PCA: ResNet and CNN-QNN exhibit similar values (6.38 % vs. 6.39 %), suggesting that both architectures compress features in a comparable manner within the first two principal components.
- Intra-Class Distance: ResNet shows a higher intra-class distance (9.96 vs. 9.80 for CNN-QNN), indicating that the melanoma image features within ResNet are more dispersed compared to CNN-QNN.
- Inter-Class Distance: CNN-QNN slightly reduces the distance between classes compared to ResNet (9.93 vs. 9.98), suggesting a better class separability.

These results indicate that CNN-QNN may offer a more compact and discriminative feature representation compared to ResNet, although the difference is not substantial. However, the lower intra-class distance of CNN-QNN may suggest a higher risk of overfitting, which should be further validated on real clinical data.

7.1. Comparative analysis with previous studies

As shown in Table 5, the proposed CNN-QNN model significantly outperforms existing approaches in the literature. While classical models such as CNN-SVM hybrids or ResNet-based architectures typically achieve accuracies between 90 % and 95 %, our hybrid quantum-classical network reaches a peak accuracy of 99.67 %. Furthermore, the precision, recall, and F1-score of our method exceed 99 %, highlighting both its sensitivity in detecting melanoma and its ability to minimize false positives.

These results demonstrate the effectiveness of quantum feature mapping in enhancing classification performance, particularly in high-dimensional and clinically relevant datasets. The inclusion of U-Net segmentation and hair removal preprocessing also contributes to the overall robustness of the pipeline. Notably, even compared to other quantum-enhanced systems, our model achieves higher classification scores, confirming the added value of our end-to-end design.

Such improvements may translate into more accurate diagnostic support in real-world dermatology settings, offering a reliable AI-based second opinion for early melanoma detection.

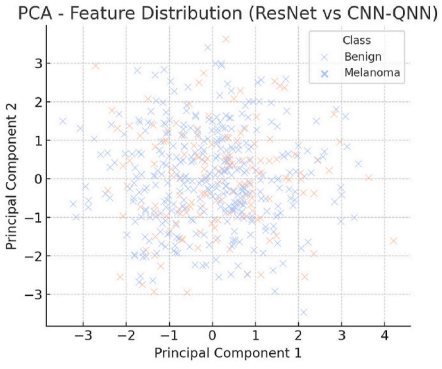

Fig. 8. Principal Component Analysis (PCA) visualization comparing feature distributions of ResNet and CNN-QNN models. The first two principal components are plotted, showing the separation between benign (blue) and melanoma (red) cases. The CNN-QNN model provides a slightly more compact representation of features, potentially enhancing classification performance.

Table 4
Comparison of PCA results for ResNet and CNN-QNN models. The table reports the explained variance, intra-class distance, and inter-class distance. Lower intra-class distance and higher inter-class distance indicate better class separability.

Model	Explained Variance (PCA)	Intra-class Distance	Inter-class Distance
ResNet	0.063778	9.960223	9.980202
CNN-QNN	0.063992	9.802606	9.931106

Table 5
Comparison of melanoma classification performance with previous studies.

Study	Accuracy	Precision	Recall
Adegun et al. (2019) [30]	90 %	–	–
Seeja et al. (n.d.)	92 %	91 %	90 %
Daghrir et al. (2020) [31]	95 %	93 %	92 %
Acosta et al. (2021) [32]	92 %	91 %	90 %
Hussain et al. (2023) [33]	95 %	–	–
Sivakumar et al. (2024) [34]	93 %	91 %	90 %
Lopez et al. (2023) [35]	94 %	–	–
Li et al. (2022) [36]	95 %	–	–
Razmjooy et al. (2020) [37]	95 %	–	–
Cirrincione et al. (2023) [38]	96 %	–	–
Proposed (CNN-QNN)	**99.67 %**	**99.35 %**	**99.67 %**

8. Discussion

This study explores the use of advanced deep learning models to analyze dermatological images, with the aim of improving the automatic diagnosis of skin lesions, particularly melanoma. By comparing U-Net models with Otsu-based segmentation techniques, it evaluates their performance using key metrics such as accuracy, precision, recall, F1 score, and AUC.

One of the standout aspects of this work is the innovative use of a hybrid CNN-QNN model. This approach takes advantage of CNNs' strengths in extracting relevant features from images and combines them with the unique capabilities of QNNs to manage complex relationships and high-dimensional data. Together, these methods create a powerful tool that outperforms traditional approaches, reducing overfitting risks, and improving generalization. The inclusion of the quantum component is particularly exciting as it opens new doors for integrating quantum technologies into machine learning.

The robustness of the model is another strong point. It consistently performs well across multiple folds of the HAM10000 dataset, highlighting its reliability in various scenarios. Clinically, this is significant—it means dermatologists could use this tool to detect melanoma more accurately and quickly, improving patient outcomes.

Additionally, its ability to integrate smoothly into existing workflows makes it an attractive option for both routine screenings and prevention programs, with the potential to reduce melanoma-related deaths.

In our study, we chose not to balance the HAM10000 dataset to preserve the clinical relevance of its natural distribution, where benign lesions are significantly more common than malignant ones. This decision reflects the real-world conditions encountered in dermatological practice, ensuring that the model is trained in a realistic context. However, this class imbalance could introduce a risk of bias, potentially reducing the model's ability to accurately identify underrepresented lesions, such as melanomas. To address this, we implemented a loss function weighting strategy that assigns greater penalties to errors involving minority classes, without altering the original data distribution. This approach allowed the model to handle the inherent imbalance effectively, maintaining its clinical applicability. Moving forward, it will be essential to validate the model on external datasets drawn from more diverse populations to assess its generalizability and identify any limitations that may arise in different clinical contexts.

Despite these strengths, the hybrid CNN-QNN model isn't without its challenges. One major limitation is the computational power required. Quantum neural networks depend on quantum computers, which are still not widely available and demand significant resources. Even simulations on classical hardware are resource-intensive, with complexity growing exponentially as more qubits are added. This limits the ability to apply these models to larger, more complex datasets.

Training these models is another hurdle. Unlike traditional neural networks, quantum circuits require tailored optimization techniques, making it harder to update weights and achieve convergence. Integrating the classical CNN with the quantum component is also tricky, as the two operate on different types of data: continuous for CNNs and discrete for quantum circuits. Balancing these differences without losing performance is no small feat.

Although the proposed hybrid CNN-QNN model demonstrated excellent performance in classifying melanoma images, it is important to acknowledge some significant limitations. First, the quantum component of the model was implemented through classical simulation, as real quantum hardware is not yet widely accessible. This entails a considerable computational burden and limits the scalability of the approach. Simulating quantum circuits becomes exponentially more demanding as the number of qubits increases, making it impractical for very large or complex datasets.

While classical CNNs are well-suited for large-scale datasets, hybrid neural networks currently face scalability challenges due to the constraints of quantum computing. At present, their applications are restricted to relatively simple problems, as only a limited number of qubits can be accurately simulated. Furthermore, the hardware requirements for training the hybrid model are not negligible. Even when executed on high-performance workstations, the addition of quantum layers significantly increases training time and memory usage. This could hinder real-world implementation, unless future advancements in quantum processors enable more efficient and scalable training pipelines. As quantum hardware continues to evolve, it may eventually become possible for hybrid models to address more complex dermatological datasets effectively.

9. Conclusion

The analysis conducted in this study has highlighted the potential of hybrid CNN-QNN models in the field of medical image analysis, particularly for the early diagnosis of melanoma. The comparison between the original dataset, Otsu-based segmentation, and the U-Net approach within the CNN-QNN framework demonstrated a clear improvement in performance across all key evaluation metrics. The integration of classical convolutional neural networks and quantum neural networks has enabled superior results compared to traditional methods, confirming the value of the hybrid approach in enhancing diagnostic accuracy and model generalization. One of the most significant aspects of our work was the improvement in dermatological image segmentation through the use of the U-Net network, which showed greater precision compared to Otsu thresholding, especially after applying hair removal techniques. The preprocessing steps, particularly the use of autoencoders and edge detection algorithms such as Canny, allowed for noise reduction and enhanced the quality of the input for the final classifier. From a computational perspective, our hybrid architecture demonstrated that introducing a quantum layer can provide a significant advantage in processing image features, improving the model's ability to distinguish between benign and malignant lesions. However, there are still limitations related to model scalability, mainly due to the difficulty of simulating quantum circuits on classical hardware and the need for access to quantum computers to fully exploit the benefits of quantum computing.

From a clinical standpoint, the proposed approach could serve as an important support tool for dermatologists, enabling faster and more accurate diagnoses. The high level of sensitivity and specificity achieved by the model could help reduce the number of false negatives, thus improving early treatment opportunities for melanoma patients. Furthermore, integrating these tools into dermatological screening programs could support a more standardized and objective diagnosis, reducing reliance on the expertise of individual specialists.

Regarding future developments, it will be crucial to test the model on larger and more diverse datasets to validate its robustness in real clinical scenarios. Additionally, optimizing the quantum component could lead to further performance improvements, particularly with the advancement of quantum hardware in the coming years.

CRediT authorship contribution statement

Maria Frasca: Writing – original draft, Methodology, Formal analysis, Data curation, Conceptualization. **Ilaria Cutica:** Supervision. **Gabriella Pravettoni:** Visualization. **Davide La Torre:** Writing – review & editing, Validation, Supervision, Conceptualization.

Ethical statement

This study was conducted in accordance with the principles outlined in the **Declaration of Helsinki** and with respect for the **ethical standards of scientific research**.

The HAM10000 dataset used in this research is a **publicly available and anonymized dataset** intended for scientific use. As such, **no ethical approval** from an institutional review board (IRB) or ethics committee was required, and **no direct involvement of human subjects** occurred during the study.

The authors affirm that all methods were carried out in **accordance with relevant guidelines and regulations**, and that all data processing complied with **privacy and data protection requirements**.

Declaration of competing interest

The authors declare that they have no known competing financial interests or personal relationships that could have appeared to influence the work reported in this paper.

References

[1] Kibbi Nour, Kluger Harriet, Nam Choi Jennifer. Melanoma: clinical presentations. Melanoma 2016:107–29.
[2] Scherer Dominique, Kumar Rajiv. Genetics of pigmentation in skin Cancer—A review. Mutat Res Rev Mutat Res 2010;705(2):141–53.
[3] Yu Zhen, et al. Early melanoma diagnosis with sequential dermoscopic images. IEEE Trans Med Imag 2021;41(3):633–46.
[4] Houghton Alan N, Polsky David. Focus on melanoma. Cancer Cell 2002;2(4):275–8.

[5] Frasca Maria, et al. A comparison of neural network approaches for melanoma classification. In: 2020 25th international conference on pattern recognition (ICPR). IEEE; 2021.
[6] Zaidi M Raza, Fisher David E, Rizos Helen. Biology of melanocytes and primary melanoma. Cutaneous melanoma 2020:3–40.
[7] Johal Kavan S, Saour Samer, Mohanna Pari-Naz. The skin and subcutaneous tissues. In: Browse's introduction to the symptoms & signs of surgical disease. CRC Press; 2021. p. 111–67.
[8] Goydos James S, Shoen Steven L. Acral lentiginous melanoma. Melanoma 2016: 321–9.
[9] McKenna Jeffrey K, et al. Lentigo maligna/lentigo maligna melanoma: current state of diagnosis and treatment. Dermatol Surg 2006;32(4):493–504.
[10] Menzies Scott W, et al. Dermoscopic evaluation of nodular melanoma. JAMA dermatology 2013;149(6):699–709.
[11] Forman Seth B, et al. Is superficial spreading melanoma still the Most common form of malignant melanoma? J Am Acad Dermatol 2008;58(6):1013–20.
[12] Meyle Kathrine Damm, Guldberg Per. Genetic risk factors for melanoma. Hum Genet 2009;126:499–510.
[13] Reichrath Jörg, Reichrath Jörg, Reichrath Sandra. Sunlight, vitamin D and malignant melanoma: an update. Sunlight, vitamin D and skin cancer 2014: 390–405.
[14] Barnhill Raymond L, et al. The biological and prognostic significance of angiotropism in uveal melanoma. Lab Invest 2017;97.6:746–59.
[15] Kasparian NA, et al. Skin cancer screening behaviours among individuals with a strong family history of malignant melanoma. Br J Cancer 2010;103(10):1502–9.
[16] Zhao Ran, et al. Implications of genetic and epigenetic alterations of CDKN2A (p16INK4a) in cancer. EBioMedicine 2016;8:30–9.
[17] Williams ML, Sagebiel RW. Melanoma risk factors and atypical moles. West J Med 1994;160(4):343.
[18] Duarte Ana F, et al. Clinical ABCDE rule for early melanoma detection. Eur J Dermatol 2021;31(6):771–8.
[19] Francese Rita, et al. An augmented reality Mobile application for skin lesion data visualization. In: 2020 24th international conference information visualisation (IV). IEEE; 2020.
[20] Ben-David S, Curigliano G, Koff D, Jereczek-Fossa BA, La Torre D, Pravettoni G, editors. Artificial intelligence for medicine: an applied reference for methods and applications. Elsevier; 2024.
[21] Pawar Karishma, Attar Vahida Z. Assessment of autoencoder architectures for data representation. Deep learning: concepts and architectures 2020:101–32.
[22] Li Pengzhi, Pei Yan, Li Jianqiang. A comprehensive survey on design and application of autoencoder in deep learning. Appl Soft Comput 2023;138:110176.
[23] Goodfellow Ian. Deep learning. 2016.
[24] Healthcare Engineering. Journal of. "Retracted: u-net-based Medical Image Segmentation.". 2023, 9890389.
[25] Schuld Maria, Sinayskiy Ilya, Petruccione Francesco. The quest for a quantum neural network. Quant Inf Process 2014;13:2567–86.
[26] Gupta Sanjay, Zia RKP. Quantum neural networks. J Comput Syst Sci 2001;63(3): 355–83.
[27] Strikis Armands, et al. Learning-based quantum error mitigation. PRX Quantum 2021;2(4):040330.
[28] Savvas Asgari, Lizarralde Mian Snell, Marsoit Patrisia Teresa. Development of quantum neural networks for complex data classification. Journal of Computer Science and Research (JoCoSiR) 2023;1(4):132–9.
[29] Shi Mingrui, Situ Haozhen, Zhang Cai. Hybrid quantum neural network structures for image multi-classification. Phys Scri 2024;99(5):056012.
[30] Adegun Adekanmi A, Serestina Viriri. Deep learning-based system for automatic melanoma detection. IEEE Access 2019;8:7160–72.
[31] Daghrir Jinen, et al. Melanoma skin cancer detection using deep learning and classical machine learning techniques: a hybrid approach. In: 2020 5th international conference on advanced technologies for signal and image processing (ATSIP). IEEE; 2020.
[32] Acosta Jojoa, Mario Fernando, et al. Melanoma diagnosis using deep learning techniques on dermatoscopic images. BMC Med Imag 2021;21:1–11.
[33] Hussain Mujahid, et al. Transfer learning-based quantized deep learning models for nail melanoma classification. Neural Comput Appl 2023;35(30):22163–78.
[34] Sivakumar M Senthil, et al. Deep learning in skin lesion analysis for malignant melanoma cancer identification. Multimed Tool Appl 2024;83(6):17833–53.
[35] Montiel Daniel A Lopez, et al. Quantum computing meets skin cancer diagnosis. In: Optics and photonics for information processing XVII, 12673. SPIE; 2023.
[36] Li Ziyi, et al. A classification method for multi-class skin damage images combining quantum computing and Inception-ResNet-V1. Frontiers in Physics 2022;10: 1046314.
[37] Razmjooy Navid, Razmjooy Saeid. Skin melanoma segmentation using neural networks optimized by quantum invasive weed optimization algorithm. Metaheuristics and optimization in computer and electrical engineering. Cham: Springer International Publishing; 2020. p. 233–50.
[38] Cirrincione Giansalvo, et al. Transformer-based approach to melanoma detection. Sensors 2023;23(12):5677.
[39] Tschandl Philipp, Rosendahl Cliff, Kittler Harald. The HAM10000 dataset, a large collection of multi-source dermatoscopic images of common pigmented skin lesions. Sci Data 2018;5(1):1–9.
[40] Pereira Pedro MM, et al. Dermoscopic skin lesion image segmentation based on local binary pattern clustering: comparative study. Biomed Signal Process Control 2020;59:101924.
[41] Nie Yali, et al. Recent advances in diagnosis of skin lesions using dermoscopic images based on deep learning. IEEE Access 2022;10:95716–47.
[42] Choudhuri Rudrajit, Halder Amiya. Brain MRI tumour classification using quantum classical convolutional neural net architecture. Neural Comput Appl 2023;35(6): 4467–78.
[43] Naidu Gireen, Zuva Tranos, Sibanda Elias Mmbongeni. A review of evaluation metrics in machine learning algorithms. In: Computer science On-line conference. Cham: Springer International Publishing; 2023.
[44] Okur Erdem, Turkan Mehmet. A survey on automated melanoma detection. Eng Appl Artif Intell 2018;73:50–67.
[45] Frasca Maria, Lin Jianyi, Torre Davide La. Comparing forward-forward and backpropagation in U-Net for melanoma image classification. In: 2024 international conference on decision aid sciences and applications (DASA). IEEE; 2024.
[46] Hakemi S, Houshmand M, Hosseini SA, Zhou X. A modified quantum-inspired genetic algorithm using lengthening chromosome size and an adaptive look-up table to avoid local optima. Axioms 2023;12(10):978.
[47] Rajaei A, Houshmand M, Hosseini SA. A dynamic programming approach to multi-objective logic synthesis of quantum circuits. Quant Inf Process 2023;22(10):384.
[48] Torghabeh FA, Hosseini SA. Deep learning-based brain tumor segmentation in MRI images: a MobileNetV2-DeepLabV3+ approach. Iranian Journal of Medical Physics/Majallah-I Fīzīk-I Pizishkī-i Īrān 2024;21(6).
[49] Frasca Maria, et al. Precision in dermatology: combining U-Net and quantum neural networks for melanoma diagnosis. In: 2024 international conference on decision aid sciences and applications (DASA). IEEE; 2024.
[50] Ahmadi Moghadam E, Abedinzadeh Torghabeh F, Hosseini SA, Moattar MH. Improved ADHD diagnosis using EEG connectivity and deep learning through combining pearson correlation coefficient and phase-locking value. Neuroinformatics 2024;22(4):521–37.
[51] Hakemi S, Houshmand M, KheirKhah E, Hosseini SA. A review of recent advances in quantum-inspired metaheuristics. Evolutionary Intelligence 2024;17(2):627–42.
[52] Jahandoost A, Abedinzadeh Torghabeh F, Hosseini SA, Houshmand M. Crude oil price forecasting using K-means clustering and LSTM model enhanced by dense-sparse-dense strategy. J Big Data 2024;11(1):117.
[53] Frasca M, La Torre D, Repetto M, De Nicolò V, Pravettoni G, Cutica I. Artificial intelligence applications to genomic data in cancer research: a review of recent trends and emerging areas. Discover Analytics 2024;2(1):10.
[54] Frasca M, Torre DL, Pravettoni G, Cutica I. Combining convolution neural networks with long-short term memory layers to predict Parkinson's disease progression. Int Trans Oper Res 2025;32(4):2159–88.